

## Infrared thermography to monitor Glare<sup>®</sup> under cyclic bending tests with correction of camera noise

by S. Boccardi<sup>1</sup>, G.M. Carlomagno<sup>1</sup>, C. Bonavolontà<sup>2</sup>, M. Valentino<sup>3</sup>, and C. Meola<sup>1</sup>

<sup>1</sup> Department of Industrial Engineering - Aerospace Division, University of Naples Federico II, Via Claudio 21, 80125 Napoli, Italy

<sup>2</sup> Department of Physics, University of Naples Federico II, Complesso MSA - 80125 Napoli, Italy

<sup>3</sup> CNR-SPIN, P.le V. Tecchio 80, 80125 Napoli, Italy

### Abstract

The capability of infrared thermography, to visualize thermoelastic effects developing in fibre reinforced composites under cyclic bending, has already been demonstrated through handy-load tests. The manual application of the load poses some problems such as the impracticality to change the load frequency and the overall test accuracy. The intention of the present paper is to carry out this investigation on fibre reinforced metal laminates by using a testing apparatus which allows power-driven load application with changing of the bending frequency. In this work, also the IR camera imaging frame rate is varied to look for the optimal value to perform tests in a quick and reliable way. Besides, a correction of the instrument and environmental noise is proposed and tested.

### 1. Introduction

Infrared thermography (IRT) has proved helpfulness in many industrial and research fields. Amongst its many applications, an infrared imaging device is useful for thermoelastic stress analysis (TSA) purposes [1], in particular, for monitoring the surface temperature change (thermoelastic effect) which is experienced by a body when subjected to volume variations under load [2]. Indeed, the thermoelastic effect was first conceived by Lord Kelvin (W. Thomson) in 1878 [3]. Many years later, in 1956 Biot [4] performed a thermodynamic analysis and formulated the classical thermoelastic equation, which expresses the change of a solid temperature ( $\Delta T$ ) in terms of the sum of its principal stresses variations ( $\Delta\sigma$ ). For isotropic materials under reversible and adiabatic conditions (i.e., in the elastic regime and neglecting heat transfer within the body and to the environment), this can be written as:

$$\Delta T = -KT_a\Delta\sigma \quad (1)$$

with  $T_a$  the absolute body temperature,  $\Delta\sigma$  the principal stresses sum variation, and  $K = \alpha/\rho c$  ( $\alpha$  thermal expansion coefficient,  $\rho$  density,  $c$  specific heat) the material thermoelastic constant. Eq. (1) relates the volume local variation to the temperature one. In particular, positive dilatation (tension) entails cooling of the material and vice-versa. On the surface of orthotropic materials, as fibre-reinforced polymers (FRP), Eq. (1) modifies (in the bulk) as:

$$\Delta T = -\frac{T_a}{\rho c}(\alpha_1\Delta\sigma_1 + \alpha_2\Delta\sigma_2) \quad (2)$$

with  $\alpha_1$  and  $\alpha_2$  the thermal expansion coefficients along the principal material directions (parallel to surface) where stresses  $\Delta\sigma_1$  and  $\Delta\sigma_2$  are respectively imposed. For complex composite materials and a more detailed analysis, it is not possible an exhaustive relationship between the mean stress and temperature variations. In any case, temperature represents an important parameter for materials dynamic characterization, and IRT represents a valuable mean for rapid determination of the fatigue limit [5]. It is worth noting that in literature the analysis is mostly driven towards the thermoplastic phase where the temperature variations are quite large making quite easy their detection. A more difficult task is to deal with measurement of unsteady temperature changes experienced by the material during the elastic phase i.e., variable thermoelastic effects.

Meola and Carlomagno first [2] tackled such a complex task; in particular, by choosing an appropriate image sampling rate, they succeeded in appraising the material temperature changes, which are due to thermoelastic effects in composites under low-energy impact. Later, Meola et al. [6] embarked upon a different measurement of thermoelastic effects generated in a cyclic beam bending. In particular, two bending configurations were considered, with the specimen loaded on one end either as a cantilever, or with a punch as central support. For both configurations, the load was manually applied, while sequences of thermal images were recorded by the infrared camera. As a main finding, it has been observed a general agreement between the local temperature changes and the bending moment distribution along the beam, while deviations of the formers were observed in presence of buried defects within the material.

The handy-load tests were useful to verify the test feasibility as well the ability of an infrared imaging system to follow temperature changes, pursuing the load variations with cooling down under tension and warming up under

compression. However, the manual application of the cyclic load poses some problems such as the impracticality to change the load frequency as well as to assure an overall test accuracy.

The purpose of the present paper is to go on in the investigation of the material behaviour under cyclic bending with infrared thermography, the main intention being to get more reliable quantitative data. Then, a testing apparatus is *ad hoc* realized to allow for a power-driven load application with changing of the bending frequency. Indeed, in this work both the bending frequency and the thermal image acquisition rate are varied in view of finding the optimal values to perform tests in a quick and reliable way.

## 2. Test setup and procedure

As sketched in Fig. 1, the test setup consists of an apparatus, which includes positioning of the specimen and application of the cyclic bending force with an electric motor via a connecting rod and a loading arm (with a trench to insert the beam free end). More specifically, the cantilever beam specimen is clamped on one side and it is free to bend under the cyclic force which is applied at the opposite end by the trench. Tests are performed by varying the bending frequency ( $f_b$ ) between 2 and 14 Hz. The specimen deflection  $D_F$  is equal to  $\pm 20$  mm, within the material elastic range, and is kept the same for all the tests. Smaller deflections do not lead to reliable temperature variation measurements.

The infrared camera can be positioned to view either the specimen top surface (by placing it above), or the bottom one with the aid of a mirror placed at  $45^\circ$  underneath the sample. The second option is herein preferred since it allows better eliminating reflections from the ambient and more easily keeping under control any disturbing effect.

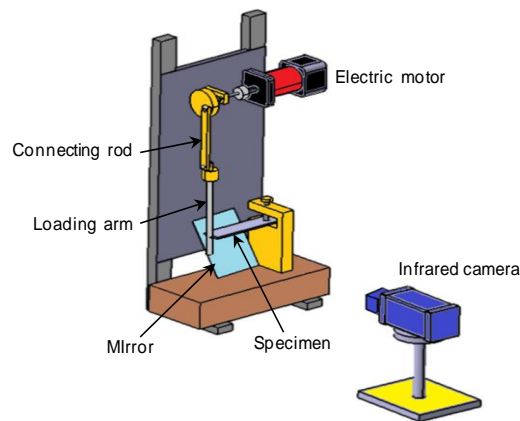


**Fig. 1.** Test setup

Specimens come from a type of fiber metal laminate (FRML) including 3 aluminum sheets with 2 glass/epoxy (GFRP) layers in between. This type of material is brand named Glare<sup>®</sup>. Specimens are 30 mm wide, 150 mm long and 1.5 mm thick and are cut from a large plate, which is fabricated following industrial standards with autoclave curing; their outside surface is covered with a green aeronautical coating having an emissivity coefficient of about 0.9.

The used infrared camera is the SC6000 (Flir systems), which is equipped with a QWIP detector, working in the 8-9  $\mu\text{m}$  infrared band, NEDT < 35 mK, spatial resolution 640x512 pixels full frame with the pixel size 25  $\mu\text{m}$  x 25  $\mu\text{m}$  and with a windowing option linked to frequency frame rate and temperature range. The imaging frame rate ( $f_{Fr}$ ) is varied from 30 Hz up to 96 Hz to look for an optimal value which may allow, at the same time, either following both temporal and spatial temperature variations and to avoid acquisition of unnecessary huge number of images.

The best camera position, identified as a good compromise between field of view and spatial resolution, ensues the possibility to view the entire specimen surface of interest with either only one frame, or more, depending on the acquisition rate. In fact, it is found that only one frame is sufficient from  $f_{Fr} = 30$  Hz to 69 Hz, two frames are required from 69 Hz to 84 Hz, while three frames are necessary for  $f_{Fr} = 96$  Hz. It has to be pointed out that, to account for variations with respect to the ambient temperature, thermal images must be taken, in time-sequence, starting before load application and ending after force removal. In addition, considering that: each test must include a certain number of loading cycles (at least 10) while - for accuracy and data repeatability - each test must be repeated at least three times in different moments, it is easy to realize the huge amount of data to deal with, when grabbing images at high frame rate. The possibility to reduce the frame rate without loss of information in terms of thermoelastic effects, thus reducing in turn the number of recorded frames to be analysed, is certainly of great importance.

## 3. Data analysis procedure

The recorded sequences of thermal images are subjected to post-processing procedures by using the Researcher<sup>™</sup> software and specific routines developed within the Matlab environment. Firstly, to account for thermal changes with respect to the ambient temperature, the first image ( $t = 0$ ) of the sequence (i.e., the temperature of the unloaded specimen surface) is subtracted to each subsequent image so as to have a map of temperature variations  $\Delta T$ :

$$\Delta T = T(i, j, t) - T(i, j, 0) \quad (3)$$

$i$  and  $j$  representing lines and columns of the surface temperature map array. Therefore, a sequence of  $\Delta T$  images is created. Such images are further analysed to bring out information on temperature variations along the specimen surface, which may be useful for material characterization. Then, as sketched in Fig. 2, several measurement positions ( $P_M$ ) are chosen, evenly distributed along the specimen length, starting about 15 mm far from the fixture ( $x = 0$ ) and moving towards the forced side, till  $x = 113$  mm. In the following, the location of such positions is, more simply, indicated in percent of the specimen length  $L$  (i.e.,  $x/L$ ). In each  $P_M$ , a data plot in time is extracted; more specifically, the resulting curve corresponds to the mean value in an area 12 pixels wide (in the  $x$  direction in Fig. 2) and which spans along the specimen width (i.e., along the  $y$  axis), by suppressing, of course, border appraisals.

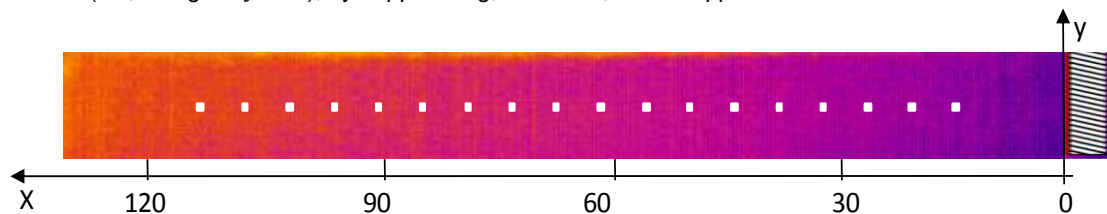


**Fig. 2.** Measurement points over the specimen surface

However, two main problems are encountered when dealing with  $P_M$  average data plots.

The first one regards the tapering effect which affects images taken, via the mirror, while the specimen bends up and down, so moving in the recorded image. This means that, to avoid edge effects, for each measurement position the average must be performed by considering areas of variable height (AVG-HV) as sketched in Fig. 3; these areas remain always within the specimen surface and are enough distant from the edges for both of the cases of maximum bending up (Fig. 3a) and bending down (Fig. 3b). Alternatively, it is possible to choose averaging areas with the same height (AVG-HS); in this case, measurement positions are enclosed in the equal areas depicted in Fig.4. Of course, the height is chosen to assure enough distance from the edges for both of the cases of maximum bending up (Fig. 4a) and bending down (Fig. 4b). The two averaging methods practically lead to the same results so only data obtained with the AVG-HS, which were simpler to perform, are reported in the following.

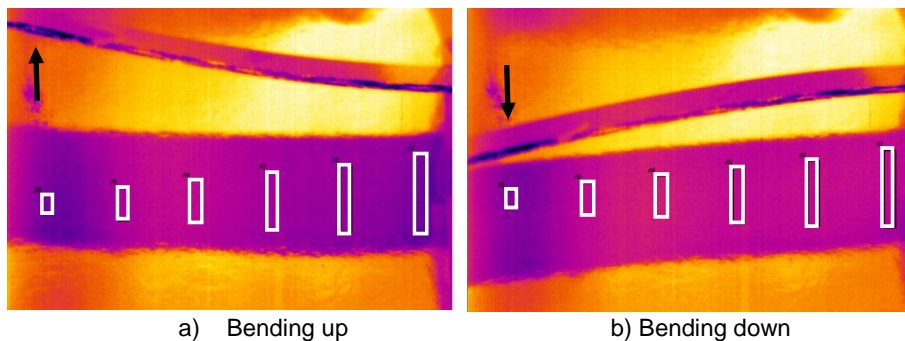


**Fig. 3.** Distribution of measurement areas of variable height

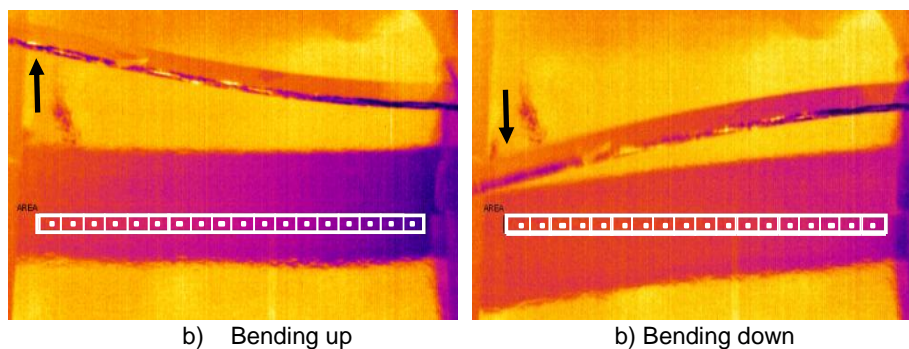


**Fig. 4.** Distribution of measurement points inside an area of fixed height

The second problem is associated with the smallness of the  $\Delta T$  values, coupled with cyclic bending, which may be affected by the instrument and environmental (temporal) noise. As an example, Fig. 5b displays three  $\Delta T$  time plots,

taken at  $f_{Fr} = 84$  Hz and  $f_b = 5.20$  Hz, in the three areas A1, A2 and A3 depicted in Fig. 5a. In these plots, it is possible to see irregularities due to temporal noise and also a signal drift is evident. Then, a specific data treatment is performed which makes use of a reference area ( $A_R$ ) for temporal noise data correction. More specifically, as sketched in Fig. 5a, the reference area is placed outside the specimen surface in an unloaded zone and its mean temperature is monitored; a plot of the output signal in  $A_R$  (which practically represents the instrument and environmental noise) is given in Fig. 5c. Then, the corrected  $\Delta T_F$  plots in Fig. 5d, are obtained from a mere subtraction of the signal of Fig. 5c from that of Fig. 5b; i.e. by calling  $\Delta T_R$  the raw signal and  $\Delta T_N$  the temporal noise, the final corrected value  $\Delta T_F$  is given by:

$$\Delta T_F = \Delta T_R - \Delta T_N \quad (4)$$

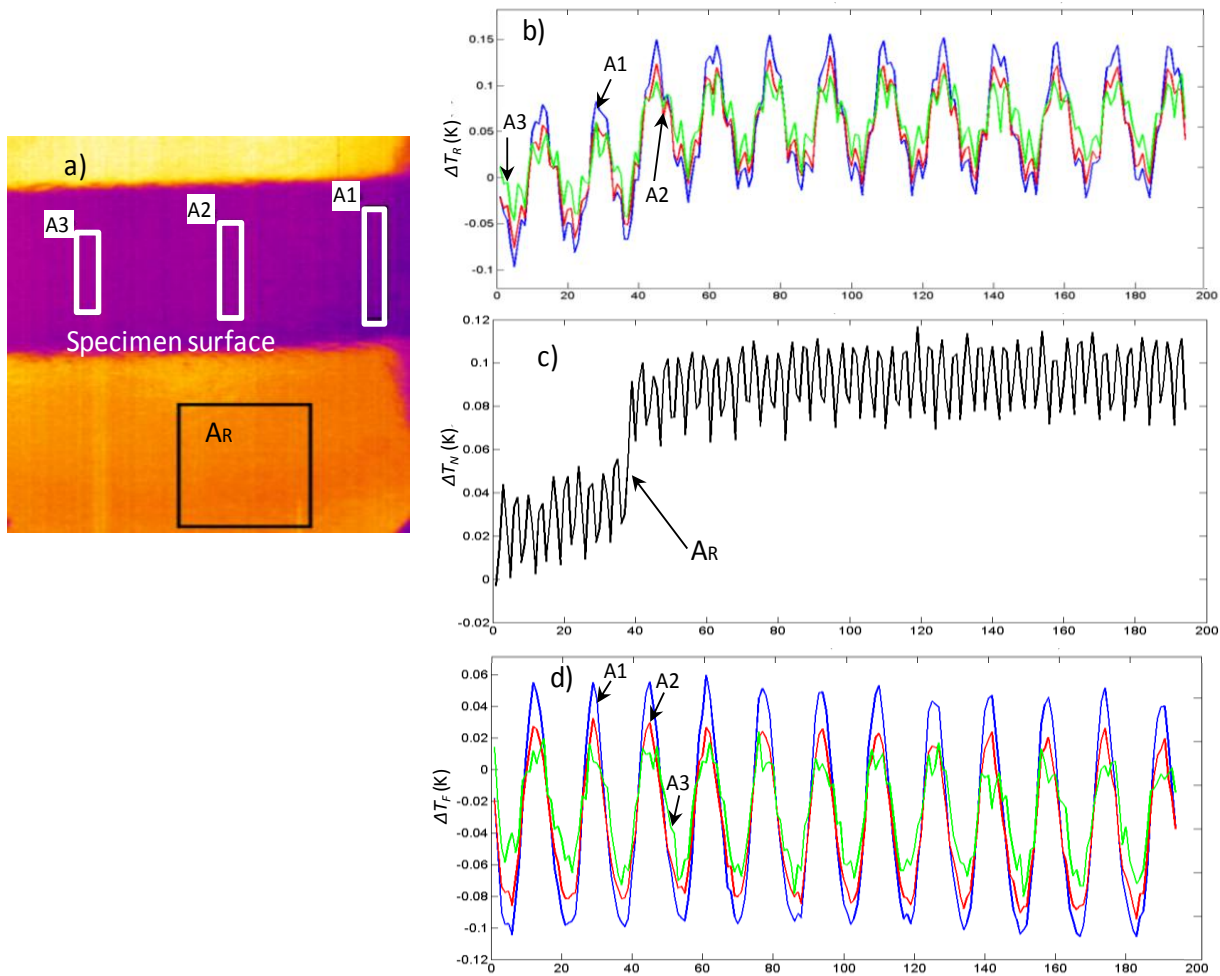


**Fig. 5.** Sketch of the signal correction procedure

By examining Fig. 5d, the adopted method of temporal noise correction looks quite effective and, to authors' knowledge, seems not to have been exploited before. Of course, the same results could have been attained by properly phase averaging the raw data.

Eq. (4) is used to correct data for all the tested conditions which will be shown in the following. In particular,  $\Delta T_F$  values in six of the afore mentioned  $P_M$  positions are shown in Fig. 6, for a fixed time interval (number of frames in the sequence) and for a given set of testing parameters,  $f_b = 5.20$  Hz and  $f_{Fr} = 69$  Hz. On the whole,  $\Delta T_F$  displays sinusoidal variations, which are perfectly coupled with the cyclic load. Of course, the sinusoidal trend is more regular for the lowest  $x/L$  value, or better closest to the specimen fixture ( $x \rightarrow 0$ ), where the bending moment attains its maximum. As  $x/L$  increases, i.e. moving towards the forced extremity,  $\Delta T_F$  decreases mingling with the left background noise of the instrument; in fact, for  $x/L = 0.83$ , the  $\Delta T_F$  distribution becomes much uneven, yet by retaining a sinusoidal fashion.

With a subsequent data processing, the  $\Delta T_a$  signal amplitude is evaluated as average value amongst a fixed number of cycles and named  $\Delta T_a$ . Values of  $\Delta T_a$  are plotted against  $x/L$  for different testing conditions in the following Figures 7 and 8, where data in the shaded areas should not be considered because very close to camera resolution.

Besides, when applying the up and down force at the beam free end, the trench may produce a small moment there that could alter the local moment distribution but have less influence where the moment values are larger.

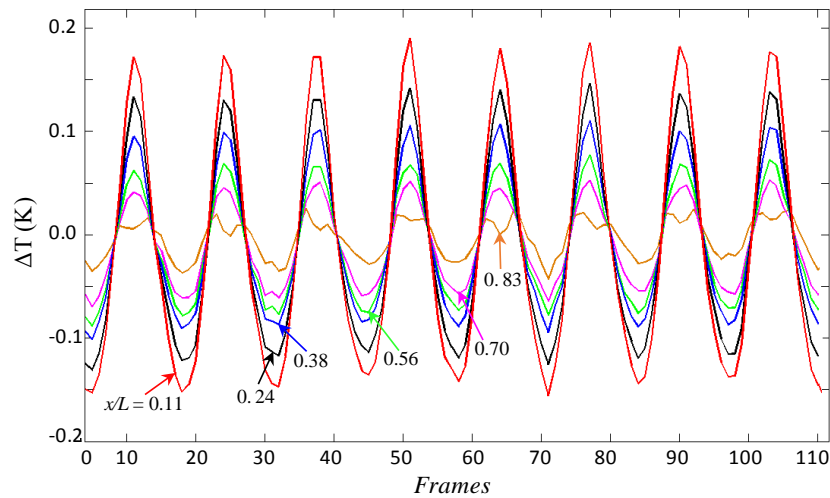


**Fig. 6.**  $\Delta T$  distribution at several positions  $x/L$  along the specimen, for  $f_b = 5.20$  Hz and for  $f_{Fr} = 69$  Hz

In particular, Fig. 7 shows a comparison of  $\Delta T_a$  values for a fixed bending frequency  $f_b = 7.25$  Hz and for frame rate  $f_{Fr}$  varying in the range 30÷96 Hz. As can be seen, in general there is a good data overlap, but it is possible to recognize that the lowest  $\Delta T_a$  values generally correspond to lower acquisition frequencies and this is consistent with the fact that, in such conditions, the detection of  $\Delta T_F$  peaks is less accurate.

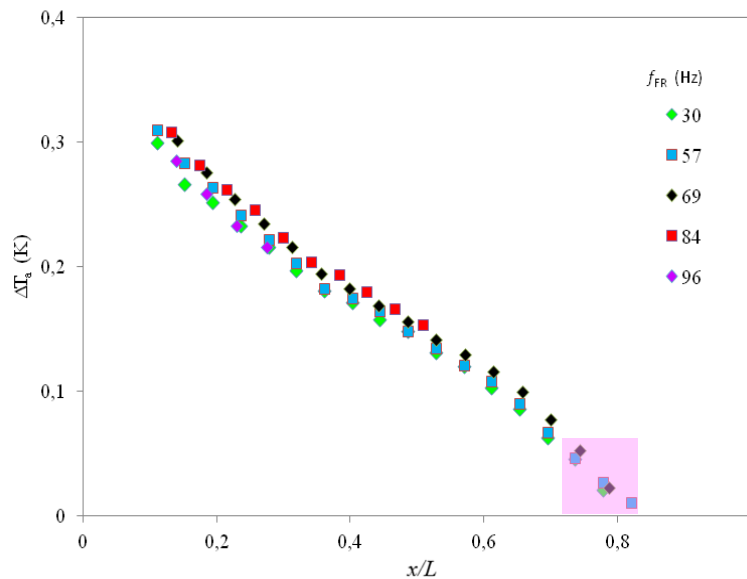


**Fig. 7.**  $\Delta T_a$  against  $x/L$  for  $f_b = 7.25$  Hz and for varying  $f_{Fr}$ .

Instead, Fig. 8 refers to  $\Delta T_a$  values for a fixed frame rate  $f_{Fr} = 69$  Hz and bending frequency  $f_b$  varying between 2.15 Hz and 13.3 Hz. In these conditions, notwithstanding the large frequency range, the data overlap is even better than for the previous ones, with no evident dependence on the bending frequency. This behaviour let to assume that the temperature variations occurring on the beam surface have not sufficient time to release underneath.

The linear trend of the central part of both diagrams of Figs. 7 and 8 shows the data tendency to attain the zero  $\Delta T_F$  value at  $x/L \approx 0.9$  and not at 1.0. It is believed that this behaviour is most probably due to the already mentioned small moment induced by the trench on the specimen free end. By considering different combinations of  $f_b$  and  $f_{Fr}$  testing parameters (including some not reported herein), it can be deduced that:

- The same temperature amplitude  $\Delta T_a$  is practically achieved independently of any value of the bending frequency at least for  $f_b$  in the range 2.15÷13.33 Hz( Fig. 8). This means that the temperature variations occurring over the beam surface have not sufficient time to release underneath.

- With regard to the frame rate, a large  $f_{Fr}$  allows better capturing the thermoelastic effects whose evolution is very fast. However for the tested bending frequencies, a good compromise, between the chance to view a large enough surface portion and chasing the temperature variations with time, has to be found.

By introducing the parameter  $R_F$  as ratio between frame rate and bending frequency:

$$R_F = \frac{f_{Fr}}{f_b} \quad (5)$$

and by considering also other tests not reported herein, it is possible to infer that the condition:

$$R_F > 6 \quad (6)$$

must be satisfied to assure chasing of thermoelastic effects developing under bending tests, at least for the material under investigation. This condition corresponds to detecting not less than about 7 frames within a single loading cycle, so as to capture  $\Delta T_a$  values with a certain confidence.

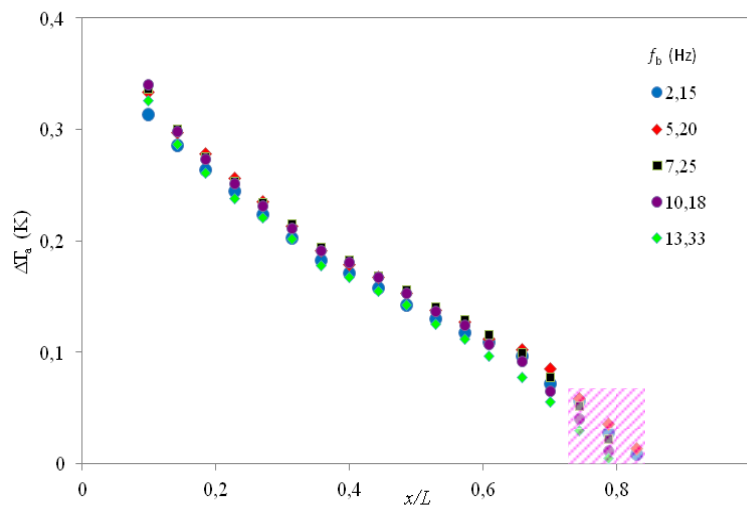


**Fig. 8.**  $\Delta T_a$  against  $x/L$  for  $f_{Fr} = 69$  Hz and for varying  $f_b$ .

#### 4. Comparison with previous work

At last, a comparison is made between present data, which are simply referred to as M-load, and the previously obtained ones [6], coming from handy-load (H-load) tests; the testing conditions are quite similar in regard of the test configuration. In fact, both data sets are obtained for a cantilever beam and taken on the bottom surface of a Glare® specimen, which is viewed by the infrared camera through a mirror. The main difference between the two data sets resides in the deflection value which is smaller ( $D_F \cong \pm 15$  mm) for H-load tests with respect to the M-load ones ( $D_F = \pm 20$  mm); besides, for H-load tests, the time evolution of  $\Delta T_F$  is quite periodical but not a sinusoidal one. In addition, M-load includes the ranges  $f_b = 2.15 \div 13.33$  Hz and  $f_{Fr} = 30 \div 96$  Hz, while H-load are restricted to  $f_{Fr} = 84$  Hz and  $f_b \approx 1$  Hz. Of course, both  $D_F$  and  $f_b$  values are rather indicative for H-load tests since their constant value cannot be guaranteed.

Notwithstanding these major differences, an acceptable general agreement is found between the two data sets, in particular, for  $x/L > 0.2$ . Instead, a larger spread is observed for  $x/L < 0.2$ , being the data for H-load quite lower than the corresponding M-load data. This may be ascribed mostly to the difference of  $f_b$  values. In fact, the bending frequency for H-load tests is much lower than those used with the M-load ones. It is worth considering that thermoelastic effects, with cooling down under tension and warming up under compression, evolve for the M-load tests in a faster manner. Then,  $\Delta T_a$  is affected by the time interval between two successive peaks.

#### 5. Conclusions

A quasi-linear dependence of the temperature amplitude  $\Delta T_a$  along the cantilever beam ( $x/L$ ) is found for all the tests. However, the intercept of the line with the  $x/L$  axis does not occur at  $x/L = 1$  but at about 0.9. This behaviour is most probably due to the small moment induced by the trench where the specimen free end is inserted. As a main finding, the obtained results are almost independent of the frame rate in the considered range 30-96 Hz, as long as the bending frequency is not too high. However, for a good choice of the frame rate it has to be considered that, at high bending frequencies, some peaks are lost at 30 Hz, which may lead to lower amplitude values and measurement errors.



Conversely, at 96 Hz the entire specimen surface cannot be visualized within a single shot, but it has to be subdivided into three zones with the need to acquire a large number of images to be recorded and analysed with also some lost in accuracy due to the successive patching up between contiguous images. Then, the frame rate of 69 Hz is found to be the best choice within the present testing configuration. However, as a general parameter, the ratio of frame rate over bending frequency is introduced, which must be greater than 6 to assure chasing of thermoelastic effects developing under bending tests.

**Acknowledgements:** The test machine (Fig.1) was fabricated with the help of Mr. Antonio Maggio and Mr. Stefano Marrazzo of the Department of Physics.

#### REFERENCES

- [1] Galietti U., Modugno D. , Spagnolo L., "A novel signal processing method for TSA applications" *Measurements Science and Technology*, Vol. 16, pp. 2251- 2260, 2005 .
- [2] Meola C., Carlomagno G.M., "Infrared thermography to impact-driven thermal effects" *Applied Physics A*, Vol. 96, pp. 759-762, 2009.
- [3] Thomson W., "On the thermoelastic, thermomagnetic and pyroelectric properties of matters", *Philosophical Magazine*, Vol. 5, pp. 4-27, 1978.
- [4] Biot M.A., "Thermoelasticity and irreversible thermodynamics" *Journal of Applied Physics*, Vol. 27, pp. 240- 253, 1956.
- [5] La Rosa G., Risitano A., "Thermographic methodology for rapid determination of the fatigue limit of materials and mechanical components", *Int. J. Fatigue*, Vol. 22, pp. 65-73, 2000.
- [6] Meola C., Carlomagno G.M., Bonavolontà C., Valentino M., "Monitoring composites under bending tests with infrared thermography", *Advances in Optical Technologies*, Vol. 2012, 7 pages, 2012.